Hindawi
Journal of Chemistry
Volume 2022, Article ID 1497117, 17 pages
https://doi.org/10.1155/2022/1497117

Research Article

Synthesis, *In Silico*, and Biological Applications of Novel Heteroleptic Copper (II) Complex of Natural Product-Based Semicarbazone Ligands

Fekadu Muleta and Tegene Desalegn

Adama Science and Technology University, College of Applied Natural Science, Department of Applied Chemistry, Adama, Ethiopia

Correspondence should be addressed to Fekadu Muleta; muletafikadu@gmail.com

Received 17 May 2022; Accepted 29 August 2022; Published 27 September 2022

Academic Editor: Marcelino Maneiro

Recently, heteroleptic coordination between essential metallic elements with semicarbazone-based derivatives attracts more consideration for the varied ranges of bioactivities. Semicarbazone-based moiety holding azomethine (C=N) group become flexible ligands, forming stable complexes. Through a stirring and reflux technique, a novel heteroleptic complex of copper (II) was synthesized by reacting two semicarbazone-based derivative ligands, ortho-phthalaldehyde disemicarbazone (L_1) and dehydrozingerone semicarbazone (L_2), with copper chloride salt in 1 : 1 : 1 molar ratio. Magnetic moment measurement, elemental analyzer, thermogravimetric (TGA) analysis, and several spectroscopic techniques were applied to describe the prepared compounds. The disc diffusion and DPPH methods were actually used to investigate the antibacterial and antiradical potentials, respectively. The obtained data indicates the ligand (L_1) has good mean inhibition zones on *Staphylococcus aureus* (12.42 ± 0.00 mm) and *S. pyogenes* (11.64 ± 0.12 mm) bacteria. The heteroleptic [Cu(L_1) (L_2)] complex displayed higher antibacterial actions (13.67 ± 0.52 mm) on *Streptococcus pyogenes* bacteria. The [Cu(L_1) (L_2)] complex also shows better antiradical potential (63.7%). Furthermore, the docking result of prepared compounds on *S. aureus gyrase* confirms the ligands (L_1 and L_2) and the complex potential molecules possess the smallest binding potential of −8.0 to −8.4 kcal/mol. A higher value was achieved by [Cu(L_1) (L_2)] complex (−8.4 kcal/mol). Thus, this study indicates an insight towards combining semicarbazone form derivatives of natural source origin with a synthetic compound as ligands through metal coordination could enhance bioactivity.

1. Introduction

Novel concepts of complex chemistry in heteroleptic complex formation involving different ligands are an important recent idea in research because of their potential biological activities. Semicarbazone derivative-based metal-coordinated substances are important and focal points in research for bioinorganic and medicinal chemistry. These derivative forms show bioactivities, mainly antiviral [1], antibacterial, fungicidal, antioxidant [2], and antiparasitic actions [3]. But a resistance developed by microbial reduces their effectiveness greatly as for potent medicinal applicants [4]. However, the ideas of coordinated complex formation with different bioactive organic ligands were an important strategy to increase the bioactivities to tackle the resistance developed and also to overcome the rising of microbial adaption to known antibiotics. Metal-coordinated compounds possess greater activity relative to pure compounds [4]. Semicarbazone-based derivatives are synthesized by condensation through refluxing semicarbazide with suitable aldehyde/ketone groups. They work as ligands possessing heteroatoms as binding modes to metals giving a stable form of complexes. The existence of metal can promote the cytotoxicity properties of coordinated semicarbazone by increasing the membrane penetration power (lipophilicity) and actions to damage bacteria cells. This is because coordinated ligands decrease the polarity and increase the nonpolarity nature of the metal [5]. The presence of the

imine bond (-C=N-) within semicarbazone ligands plays a central role in the antibacterial mechanism of action [6]. Thus, to synthesize semicarbazone-based derivative ligands for heteroleptic complex formation, natural product origin (dehydrozingerone) and synthetic origin (ortho-phthalaldehyde) [7] were purposely focused on. Ortho-phthalaldehyde (OPA) contains two aldehyde groups that are proposed for antimicrobial action [8]. However, practically all bacteria species gain increasing resistance to its activity almost immediately [8]. It reacts with amine-containing molecules [9, 10]. Dehydrozingerone is a ketone-containing natural substance identified in the traditionally used medicinal herb ginger (Zingiber officinale) [11, 12]. These facts motivated us to develop ligands from semicarbazone-based derivatives of ortho-phthalaldehyde, dehydrozingerone, and their heteroleptic copper (II) complex to a higher extent as potent bioactive ancillary compounds, to tackle multidrug-resistant microbial pathogens.

The pharmacological studies which are a crucial tool in the current drug investigation [13, 14] were performed for the synthesized sample compounds. It comprises characteristics that are effective in identifying key bioactive compounds, such as drug-likeness, ADME, and toxicity [14]. Selecting bioactive compounds has recently been easier to *in silico* techniques like docking and online ADMET predictions (Swiss ADME, Pro-Tox II, and OSIRIS property explorer) [15–17] and also to support experimental results.

Thus, a synthesis, antibacterial, antioxidant, *in silico* docking studies, and drug-likeness evaluations of novel heteroleptic copper (II) compounds incorporating OPA-disemicarbazone, and dehydrozingerone-semicarbazone ligands were reported. The goal was to see how effective they were as new compounds for antibacterial and antioxidant agents created by coordinating different bioactive ligands with copper (II) metal.

2. Experimental

2.1. Materials and Methods. Analytical-reagent (AR) grade chemicals, reagents, and standard instruments were used. Semicarbazide hydrochloride, sodium acetate, glacial acetic acid, ortho-phthalaldehyde (OPA), dehydrozingerone, metal salts, methanol, diethyl ether, and ethanol were received from Alchem Pvt. Ltd., Addis Ababa. Stuart SMP^3, an electrothermal device made in the UK, was used to measure the melting points of the samples. The purity of samples during synthesis was checked by TLC run by UV254. Using a Chem LAB UV spectrometer, an absorbance measurement for the samples was made in the UV/Vis range (scan wavelength: 200.0–800.0, test mode: ABS mode) nm. The CHN analyzer performed elemental assays for C, H, and N and also together with the metal by SEM-EDX. A Perkin Elmer FT-IR spectrophotometer (400–4000 cm^1), model no. BX, was used to record the FT-IR spectra data as KBr pellets. A Bruker advance 400 spectrometer running at 400 MHz was used to gather the NMR spectra data in DMSO-d_6. The XRD data were determined by Philips X-pert pro diffractometer, PW 1830. The weight loss vs temperature relationship is measured by the TGA-60H thermal analyzer. While N_2 gas was present, the scanning was performed at a rate of 10.0 degrees per minute, until 1500 K.

2.2. Synthesis of Ortho-Phthalaldehyde Disemicarbazone Ligand (L_1). The semicarbazone moiety was prepared by following the condensation through the refluxing technique, from the raw materials ortho-phthalaldehyde and salt form of semicarbazide (Figure 1), by adopting a similar method used by Deluchat [7] and Goel et al. [18].

The semicarbazide with hydrochloride (0.01 mol and 1.11 g) prepared in 30 mL aqua ethanol was mixed with 30 mL ethanol solution of ortho-phthalaldehyde (0.005 mol and 0.67 g) together with CH_3COONa (0.01 mol and 0.82 g).The semicarbazide were generated from semicarbazide hydrochlorides by CH_3COONa. The CH_3COOH produced during the reaction progress protonates the C=O functional group of ortho-phthalaldehyde. As a result, the carbon atom has a greater ability to undergo a nucleophilic reaction. The clear solution formed was continuously stirred through refluxing at 65–70°C for around two hours. The completion and product formation were checked by spot detection using TLC. The crude product obtained was filtered, washed repeatedly with ethanol and warm water, and then dried under a vacuum desiccator over P_4O_{10}. Yield: 75%, color: cloudy powder, m.p = 240–242°C, and Rf = 0.41 (EtoAc: methanol = 7 : 3). Elemental analysis for $C_{10}H_{12}N_6O_2$, (Mwt. = 248.24): Calc. %; C = 48.34, H = 4.83, N = 33.83, found; C = 47.86, H = 4.64, N = 34.02. UV-Vis (DMSO) λ_{max}(nm) = 282 and 314.4. FT-IR (υ cm^{-1}, KBr): 3372 υ (1° N-H), 3203.4 υ (N-H), 3055.4 υ (Ar-C-H), 2922.4 υ (aliph C-H), 1862 υ(aromaticity), 1688.5 ν (C=O), 1583 ν (C=N), 1505.4 ν (arom C=C), 1088.6 ν (C-N), ^{1}H NMR (DMSO-d_6, ppm, 400 MHz): δ = 10.44 (s, 2H, H_5), 8.33 (d, 2H, H_4), 7.87 (dd, 6.0, 3.4 Hz, 2H, H_3), 7.37 (s, 2H, H_2), 6.50 (s, 4H, H_1). ^{13}C NMR (DMSO-d_6, 101 MHz), δ_c = 157.2 (C-5), 138.9 (C-4), 132.4(C-3), 129.3 (C-2), 128.3(C-1). ^{13}C-Dept-135 (ppm, DMSO-d_6, 101 MHz) δ_c = 138.9 (C-4), 129.3(C-2), and 128.3 (C-1).

2.3. Synthesis of Dehydrozingerone Semicarbazone Ligand (L_2). Semicarbazide in hydrochloride form (1.12 g) and CH_3COONa (0.82 g) by equimolar (0.01 mol) were mixed and dissolved in 30 mL distilled water within a beaker. The mixture was warmed in an oil bath up to the observation of a clear solution releasing semicarbazide from its salt form (Figure 2). Dehydrozingerone as a starting material (1.92 g) dissolved by methanol (25 ml) was gently transferred drop-by-drop to the homogenous solution and heated to the point of reflux at 70–75°C. A catalytic amount of hydrochloric acid (drop-wise) was steadily introduced in a bath under reflux for 4 h until the reaction was completed. The progress and reaction completion was confirmed by thin-layered chromatography. The final product was then refrigerated on ice, filtered, dried in vacuum desiccators, and then redissolved and crystallized from ethanol to avoid unreacted species [19]. Yield: 78.5%; color: brown powder, m.p = 170.5°C, and Rf = 0.60 (EtoAc: methanol = 7 : 3). Elemental composition for $C_{12}H_{15}N_3O_3$ (Mwt. = 249.27), Calc. %; C, 57.8; H, 6.1; N, 16.9.

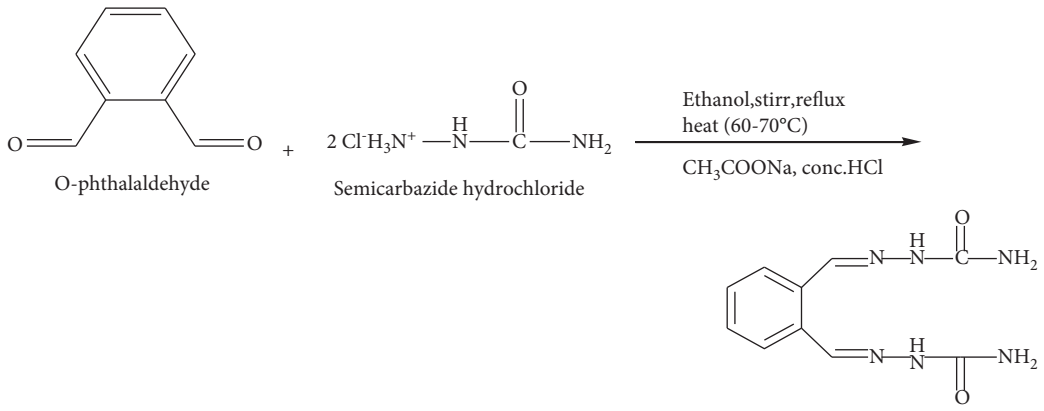

Figure 1: proposed synthesis path of L_1.

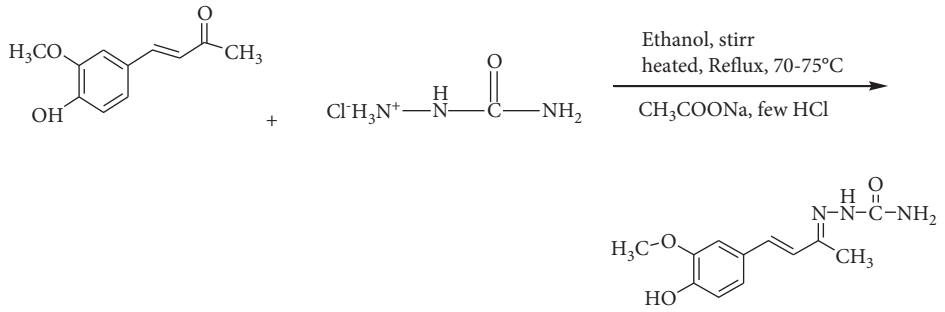

Figure 2: proposed synthesis path of L_2.

Found %; C, 57.7; H, 5.8; N, 16.2. UV-Vis (MeOH) λ_{max} (nm): 209 and 333 (figure S2). FT-IR (υ cm^{-1}, KBr): 3578 υ (O-H), 3485–3204 υ (N-H), 2929 υ (arom C-H), 2852 υ (aliph C-H), 1695.7 υ (C=O), 1583 υ (C=N), 1509 υ (arom C=C), and 1437 υ (O-H bend). A ^{1}H NMR (DMSO-d_6, 400 MHz), δ/ppm: 2.01 (s, H-1), 3.80 (s, H-2), 6.44 (s, H-3), 6.75–6.83 (d, H-5, H-6, J = 8.2 Hz), 6.94 (s, H-8), 6.85 (d, H-4, J = 16 Hz), 6.93 (d, H-7, J = 16 Hz), 9.28 (s, H-9), and 9.35 (s, H-10). ^{13}C NMR (DMSO-d_6, 101 MHz) δC: 11.97 (C-1), 55.97 (C-2), 110.22 (C-3), 116.07 (C-4), 120.85 (C-5), 127.01 (C-6), 128.59 (C-7), 132.23 (C-8), 146.67 (C-9), 147.46 (C-10), 148.29 (C-11), and 157.7 (C-12). ^{13}C-Dept (DMSO-d_6, 101 MHz) δC: 11.98 (C-1), 55.99 (C-2), 110.24 (C-3), 116.10 (C-4), 120.26 (C-5), 127.01 (C-7), and 132.24 (C-8).

2.4. Synthesis of Heteroleptic Cu(II) Complex. $CuCl_2.2H_2O$ (0.001 mol, 0.17 g), a copper salt, was added and dissolved in 30 mL ethanol. Then, by swirling magnetically during heating in a bath, 30 mL ethanol solution containing ortho-phthalaldehyde disemicarbazone (0.001 mol, 0.19 g) and dehydrozingerone semicarbazone (0.001 mol, 0.25 g) ligands were added together. Then, it was refluxed at 75–80°C temperature for five hours till the color change appeared. The pH of the mixture was kept at around 7.5–8 pH by adding 5% of NaOH solution through stirring for 30 minutes. The end of the reaction was confirmed by TLC, and then the contents were cooled and the precipitate formed was filtered, washed with hot water, ethanol, and recrystallized in ethanol, then put in a desiccator over $CaCl_2$ to remove moisture and dried. Then, the dried substance was preserved in a clean vial for further analysis.

2.4.1. Copper Complex. [Cu(L_1) (L_2)]; Yield: 54.6%; color: brown crystal and m.p > 300°C. Elemental analysis for $C_{22}H_{25}N_9O_5Cu$ (Mwt. = 559.01) calculated %: C, 47.23; H, 4.47; N, and 22.54, found % = C, 46.86; H, 4.23; N, 21.98. UV-Vis: λ_{max} (DMSO) = 333.4 nm. FT-IR (KBr, υ cm^{-1}): 3404 υ (O-H), 3267, 3146 υ(N-H), 2926 υ (arom C-H), 2851 υ (alph C-H), 1517 υ (C=N), 1504 υ (arom C=C), 1361 υ (asy C-O-C), 1023 υ (sym N-N), 538.4 υ(M-N), and 447.5 υ (M-O). TGA mass loss 44.5% (225.2–313°C, 1st step, calc.1 × $C_{10}H_{12}N_6O_2$ = 248.8 g), 5.6% (387.3–413.9°C, 2nd, $CH_3 + NH_2$ = 31.3 g), and 21.8% (497.4–586.8°C, 3rd step, 1 × $C_7H_7O_2$ = 122.9 g). Molar conductance (λ_m) = 16.4 $\Omega^{-1}\cdot cm^2\cdot mol^{-1}$. Magnetic moment: 2.18 BM.

2.5. Antibacterial Evaluation. Appling the disc diffusion method, the potential of the samples to inhibit bacterial from growth was examined against four Gram-positive and Gram-negative bacterial species, including *Streptococcus pyogenes*, *Staphylococcus aureus*, *P. aeruginosa*, and *E. coli*. [19, 20]. The media applied for bacteria's growth were made following the previously reported method using Mueller–Hinton agar (MHA), which is a suitable medium for the growth and susceptibility test of bacteria and together with molten nutrients, which also help support bacterial growth. DMSO was taken to be a negative control, and trimethoprim as positive control. Two distinct concentrations (100 and

200 g/mL) of the samples were used for testing on the bacterial species. The 6 mm diameter size of paper discs were soaked with 1 mL solution of prepared compounds. The sample-soaked paper discs were placed on duplicate bacteria-growing dishes. The dishes were left at 35–37°C for around 18 hours. Then, the distance moved by the chemicals inhibiting bacteria growth was measured to evaluate the observed zone that emerged around the disc. In triplicate experiments, the distance of inhibition zone was determined, and an average was calculated.

2.6. Antioxidant Evaluations. By using the diphenylpicrylhdrazyl (DPPH) method, the radical foraging capability of the samples was examined [19]. diphenylpicrylhdrazyl was dissolved by DMSO to prepare 0.04 mg/mL concentration and a 1 mL amount was transferred to a 4 mL solution of the sample in DMSO to prepare varied concentrations of 12.5, 25, 50, and 100 μg/mL, and control was made by pouring DPPH (1 mL) in 4 mL DMSO, and 4 mL DMSO was considered as blank. The UV-Vis spectrophotometer found in the Chem Lab was used for absorbance measurement at 517 nm after each solution was shaken and placed under a dark oven for about 30 minutes [3]. Vitamin C as standard was made at varied concentrations similar to the samples. The DPPH radical scavenging activity was calculated using the following formula [21]:

$$\text{DPPH radical scavenging potential (\%)} = \frac{\text{Control} - \text{Test}}{\text{Control}} \times 100, \quad (1)$$

where control is the absorbance of DPPH solution without the sample compounds and Test is absorbance of the sample with the DPPH solution.

2.7. In Silico Molecular Docking Studies. ChemDraw was used to create two-dimensional structural orientations for the produced compounds. The cofactors were modified during the optimization process to achieve a desirable stable structure possessing minimum energy. A 2D and 3D geometry for the prepared compounds was created using a straightforward structural optimization approach [16]. From the protein data bank, the specific structure of bacterium enzyme or human myeloperoxidase was loaded. Protein was produced using AutoDock 4.2.6 to eliminate the cocrystallized substrate, water, and contaminants, as per the present standard synthesis methodology (MGL 1.5.6). The grid box for docking against *S. aureus* was adjusted with this application. Myeloperoxidase, a bacterium enzyme, and chemicals in protein reactive sites were transported using AutoDock Vina [16]. The lattice packet was created by 20, 20, and 20, pointing in the *x*, *y*, and *z* directions, respectively, with a grid point spacing of 0.375 Å. The center grid box was set at 62, 30, and 62 Å for 2XCT and 65, 40, and 65 Å for the *x*, *y*, and *z* centers, respectively, whereas for docking against *P. aeruginosa*, a grid box was constructed using 50, 50, and 50 in the *x*, *y*, and *z* dimensions with grid-center values of 20.398, 13.779, and 77.711 Å for the *x*, *y*, and *z* centers, respectively. In both cases, the total number of genetic algorithms was set at 100, which generated one hundred different conformations for each of the molecules. For all atoms, standard docking parameters were used. After docking, the conformers with the lowest binding free energies were used for the visualization of the interactions between the active amino acids and the molecules using Discovery Studio software.

The primary pharmacokinetic parameters were created using the Swiss ADME tool. It provides details on potential bonding and the overall polarity of the compounds. The compounds' toxicity was evaluated following Lipinski's rule, and preADMET predictors were used to estimating both toxicity properties and LD50 [15, 16]. The data gained were compared with trimethoprim and ascorbic acid as standards.

2.8. Statistical Analysis. The analysis of the bioactivity data was conducted in triplicates and the results were given as mm (mean SD of triplicates). Using the ANOVA test, with an acceptable significance value of $p < 0.05$, the obtained data were tested for significant differences.

3. Results and Discussion

The aldol condensation through reflux methods were applied to successfully synthesized semicarbazone-based derivative ligands (L_1 and L_2) and their novel Cu(II) complex compound. The imine (-C=N-) bond formation, which is the main indication for the formation of semicarbazone-based derivative ligands was created by interacting the amine component of the semicarbazide with ketone and aldehyde groups (C=O) to yield imine (-C=N-) holding derivatives. Semicarbazide is released from semicarbazide hydrochloride when the reagent CH_3COONa is introduced during the synthesis process. The acid (CH_3COOH) produced when the reaction occurs, hydrogenates the oxygen of ortho-phthalaldehyde and dehydrozingerone and activates the C=O carbon favorable to nucleophilic reaction [22]. In solvents like water, methanol, and ethanol, the samples were only slightly dissolved; however, within DMSO all the compounds were completely dissolved.

3.1. Conductivity of the Complex. The conductivity value of [Cu(L_1) (L_2)] in 10^{-3} M DMSO was 16.4 $\Omega^2 \cdot cm^2 \cdot mol^{-1}$, showing that the heteroleptic complex was nonelectrolyte, as a conductivity value below 60 $\text{ת}^{-1} \cdot cm^2 \cdot mol^{-1}$ is standard values for nonelectrolyte substance dissolved in DMSO [23]. Hence, no ions were detected at the exterior coordination complex. The value obtained may be due to DMSO, which can act as a binding solvent resulting the solvolysis process [23]. The resulting complex was proposed to be formulated as [M(L_1) (L_2)$X_2(H_2O)_n$], M = Cu, L_1,L_2 = ligands, and $X = Cl^-$.

3.2. The UV-Vis Spectra Analysis. The UV-Vis spectra for the synthesized compounds were generated by dissolving in dimethyl sulphoxide and measured in the range of 200–800 nm. The observed band of L_1 indicated by Figure S1 (see supplementary materials) shows peaks around 282.2 and 314.5 nm. The observed peak at 282.2 nm confirms the

$\pi-\pi*$ transition for the cyclic (benzene) ring and the peak at 314.5 nm was attributed to $n-\pi*$ transitions of nonbonding electrons that exist on the nitrogen atom (-HC=N-). The L_2 spectra band shows two peaks: one observed at 309.4 nm for the $\pi-\pi*$ transition of an electron in the aromatic ring [19, 24] and at 333 nm for the $n-\pi*$ transition of lone-pair electrons found on the nitrogen atom (Figure S2) [25, 26]. The complex showed only one spectra band that underwent a blue or red shift as compared with the ligands (Figure S3). Regular octahedral copper (II) complexes often exhibit a single wideband over 10,000 cm^{-1}, which is a $^2E\_\_^2T_2$ transition [27]. Thus, the newly synthesized Cu (II) complex showed one absorption peak around 340.4 nm which is endorsed for $^2E\_\_^2T_2$ transitions of octahedral geometry.

3.3. FT-IR Spectra Analysis. The FT-IR spectrum data are crucial tools for determining the stretching and vibrational frequencies of bonding groups that exist in compounds. The extent of complex formation from the respective ligands can be confirmed by relating their FT-IR data of spectrum as indicated in Figures 3–5. The main group confirming the real formation of L_1 and L_2 was characterized by the appearance of the imine (C=N) group. The v(C=N) for L_1 and L_2 ligands were found at 1582.9 cm^{-1}, while v(C=N) for the [Cu(L_1) (L_2)] complex was at 1524 cm^{-1}. This indicates the shift of frequencies by 58.9 cm^{-1}, confirming that both L_1 and L_2 ligands were coordinated by the nitrogen of the imine group [28]. Similarly, v(C=O) for L_1 and L_2 were indicated at 1688.5 and 1695.5 cm^{-1}, respectively, but in [Cu(L_1) (L_2)], it was observed at 1602 cm^{-1}, lowered by 86.5 and 93.5 cm^{-1}. This confirms the binding of ligands to copper by the oxygen atom. In addition, the appearance of new week bands between 538.4 and 447.5 cm^{-1} is ascribed to v(M-N) and v(M-O) coordination [24] (Figure 5).

3.4. Elemental Analysis. The elemental composition of the compounds was generated from the CHN and EDX analysis results. The EDX spectra of the [Cu(L_1) (L_2)] complex showed characteristic signals of carbon, nitrogen, oxygen, and copper. It indicates the complex is composed of CHCuNO (Figure 6). The EDX data of the complex confirms that the ligands were in a complex with copper in the sample. The calculated values were close to found (experimental) values. Furthermore, SEM was done to study the morphology and size of the crystal of the complex (Figure 7). The SEM image showed the crystallinity of particles in the complex. Thus, both the SEM image and XRD results confirm the complex has a crystalline-like structure.

3.5. NMR Data Analysis. The evidence for structural elucidation of ligands was also confirmed using both ^1H and ^{13}C-NMR together with ^{13}C DEPT-135 data, which provides precise information about the exact positional and number of proton and carbon atom species of proposed structures. Signal protons around 6.5 and 7.37 ppm on the ^1H NMR spectra of L_1 were assigned to NH_2 (H_1) and NH (H_2) protons, respectively. CH (H_3) and (H_4) protons were also detected at 7.87 and 8.33 ppm, respectively. The signal proton around 10.43 ppm validates the N=CH (H_5) proton, indicating that the L_1 ligand was perfectly synthesized (Figure 8).

The ^{13}C-NMR graph of L_1 indicated a signal found at 157.2 ppm allotted for carbon in (C=O), and a signal for carbon in (C=N) was found at 138.86 ppm. Other remaining signals observed at 128.3, 129.3, and 132.4 ppm were for carbons found on the cyclic ring, which perfectly matched the proposed structure (Figure 9).

The proton signals found around 2.01 and 3.89 ppm for L_2 are ascribed to protons of the OCH_3 (methoxy) group and $-CH_3$ bound to imine carbon, respectively [19]. The carbothioamide (NH_2) group proton signal is observed at 6.44 ppm. The other signals observed at 6.93 and 6.71 ppm were for ethylene group protons. The O-H and N-H protons were indicated at 9.28 and 9.35 ppm. Signals for the aromatic protons appeared at 6.94, 6.83, and 6.75 ppm as indicated in Figure 10. Furthermore, the ^{13}C-NMR graph of the L_2 ligand indicated a signal observed at 157.7 ppm for a carbonyl (C=O) carbon, and the carbon signal of imine (C=N) was located at 148.29 ppm. The carbons of the benzene ring attached to OCH_3 and OH were observed at 147.47 and 146.66 ppm, respectively. The aliphatic (CH=C-H) carbon signals were located at 132.23 and 128.59 ppm [29]. The other signals for carbons in the ring were observed at 127.01, 120.85, 116.07, and 110.22 ppm, and the carbon signals for methoxy and methyl groups were indicated at 55.97 and 11.97 ppm (Figure 11). So, the data obtained best match the proposed structure.

3.6. Thermogravimetric Analysis of Cu(II) Complex. For metal complex compounds, the TGA, DTA, and DTG graphs provide useful geometrical data. TGA was used to approve the presence/absence of coordinate or hydrate water molecules found in the complex chemical. There is no mass loss in the thermogram graph of the heteroleptic copper (II) complex until it reaches 225°C, showing that there is no coordinated water molecule. In the first stage of breakdown, coordinated components of either L_1 or L_2 ligand are released from the complex. The collected TGA/DTG/DTA data are presented in Table 1, and the corresponding thermogram curves are shown in Figures 12 and 13.

The TGA curve of [Cu(L_1) (L_2)] complex indicates its stability until 225.2°C. It showed a mass loss of 44.5% (cal. 44.4%) within 225–314°C with a DTA peak found at 292°C. This decomposition stage confirms releasing of coordinated L_1. The other ensuing steps at the second and third weight losses were 5.6% and 21.8%, respectively, totaling 27.4% (cal. 26.5%) in between 329 and 586.4°C confirming a releasing of some fragmented portion of dehydrozingerone. The remaining part was metal residue above 586.4°C.

3.7. The XRD Characterization Study. The complex sample was analyzed at 37°C by an X-ray diffractometer with Cu Kα radiation. The XRD array of [Cu(L_1) (L_2)] complex as shown in Figure S4 confirms the crystallinity of the complex. It was recorded at 2θ ranging from 10–80° at a lambda (λ) value at

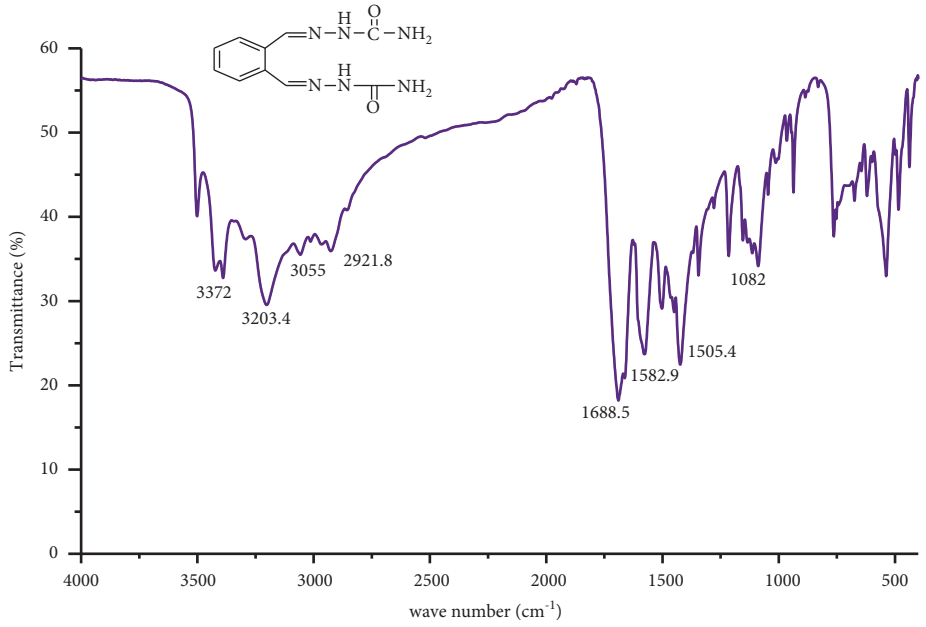

Figure 3: The FT-IR spectra of L_1.

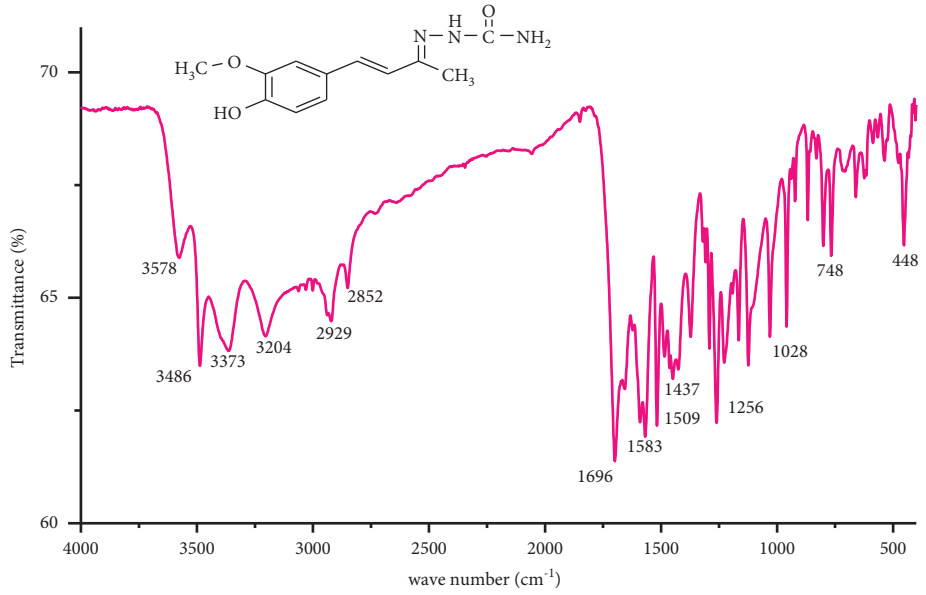

Figure 4: The FT-IR spectra of L_2.

1.54 Å. The diffractogram for the complex showed ten reflections with maxima at 2θ (27.26 Å) equivalent to a d-value of 2.619 Å. The size of the crystal was calculated using Scherer's formula ($Cs = K\lambda/\beta 2\theta \mathrm{COS}\theta$), Cs = crystal size, k is constant ($k = 0.94$), $\beta_{2\theta}$ width at half maxima of all peaks by the XRD array, λ is a wavelength used ($\lambda = 0.154$ nm) while θ is Bragg angle. Then, diffraction arrays were successfully done by a computer program. Accordingly, the size of the crystal of the novel mixed copper complex obtained was 46.72 nm.

Thus, according to the characterization findings, the produced complex was written as [Cu(L_1) (L_2)]. As a result, a structure for the synthesized complex was postulated based on spectral studies, elemental analysis, SEM-EDX, XRD, magnetic investigations, TGA data, and physical parameters (Figure 14).

3.8. Antibacterial Evaluations. The bioactive imine (-N=CH-) group in semicarbazones as an organic ligand is what gives them their main biological activity. The imine group facilitates different mechanistic actions in biological systems. It makes the semicarbazone-based derivatives active in a living system. Hence, in order to create the best

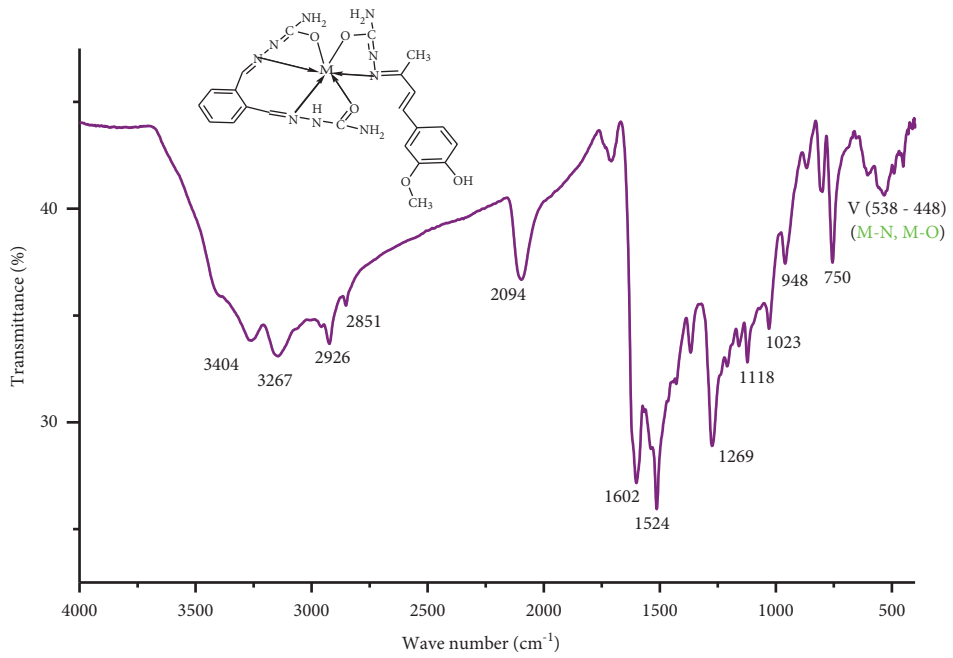

Figure 5: The FT-IR spectra of [Cu(L_1) (L_2)] complex.

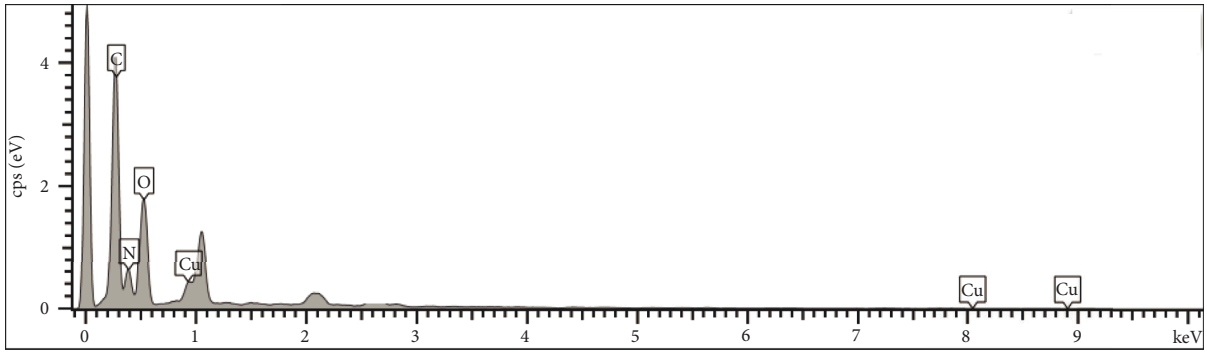

Figure 6: EDX spectra of [Cu(L_1) (L_2)] complex.

Table 1: Thermogravimetric analytical data of the complex.

Complex	Temp of TGA (°C)	Temp DTG (Endo)	Weight loss (%)		Assignments	DTA temp (°C) endo. peaks
			Calc	Found		
[Cu(L_1) (L_2)]	(1) 225.2–313.9	291.2	44.4	44.5	Loss of ligand L_1	292
	(2) 328.9–417.2	396.7	5.5	5.6	Loss of NH_2 and CH_3	
	(3) 497.4–586.8	516.2	21.0	21.8	Loss of fragmented L_2	

bioactive drug candidates vs. bacterial species, the synthesized sample ligands and their complex were tested for antibacterial activity, and the results are presented in Table 2.

The data revealed that the samples had medium to higher activities on the bacteria strains. L_1 shows a higher mean distance of inhibition on *S. aureus* bacteria (12.42 ± 0.23 mm at 200 μg/mL). The complex [Cu(L_1) (L_2)] showed higher activity on *S. pyogenes* (13.67 ± 0.52 mm at 200 μg/mL) than the ligands and was comparably relative to trimethoprim (16.71 ± 0.77 mm). It also displayed that a complex showed higher results than the constituent ligands for all bacteria strains at similar concentrations. The obtained data conclude that metal complexed to bioactive ligands enhances their activities to inhibit bacterial progression and induces potential for growth inhibition. Furthermore, the activity of all

Table 2: Antibacterial activity results of the compounds.

Compounds	Conc. (μg/mL)	Gram-negative		Gram-positive	
		E. coli	*P. aeruginosa*	*S. aureus*	*S. pyogenes*
L_1	100	8.00 ± 0.21	7.35 ± 0.42	10.52 ± 0.22	9.23 ± 0.46
	200	9.40 ± 0.42	8.33 ± 0.37	12.42 ± 0.23	11.64 ± 0.12
L_2	100	4.50 ± 0.24	3.50 ± 0.00	6.34 ± 0.42	6.64 ± 0.47
	200	5.44 ± 0.54	7.33 ± 0.46	8.68 ± 0.32	8.84 ± 0.32
[Cu(L_1) (L_2)]	100	9.20 ± 0.44	10.46 ± 0.44	11.67 ± 0.25	12.44 ± 0.22
	200	11.12 ± 0.54	12.43 ± 0.23	12.62 ± 0.34	13.67 ± 0.52
Trimethoprim (standard drug)	100	14.69 ± 0.47	16.64 ± 0.48	14.05 ± 0.44	16.71 ± 0.26

Note:-mean ± SD of triplicates is measured in mm, where SD = standard deviation.

Table 3: percentage of antiradical activities of the compounds.

Compounds	Conc. in μg/mL			
	12.5	25	50	100
L_1	32.60 ± 0.42	35.34 ± 0.22	36.67 ± 0.44	40.34 ± 0.24
L_2	36.00 ± 0.45	37.04 ± 0.48	37.08 ± 0.45	41.46 ± 0.47
[Cu(L_1) (L_2)]	60.44 ± 0.52	60.74 ± 0.46	61.32 ± 0.47	63.7 ± 0.24
Ascorbic acid	85.6 ± 0.44	86.44 ± 0.28	87.46 ± 0.58	88.48 ± 0.37

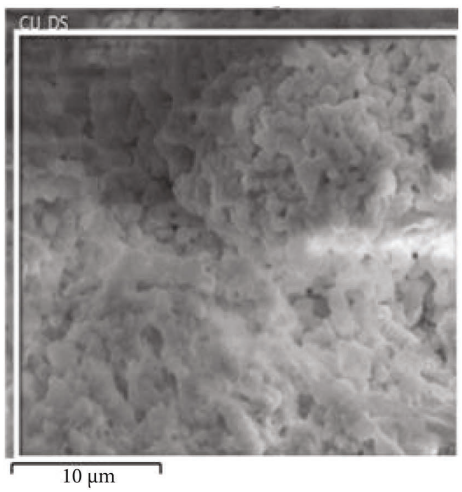

Figure 7: SEM image of [Cu(L_1) (L_2)] complex.

the samples was directly proportional to their concentration (Figures 15 and 16).

3.9. Antioxidant Evaluations. The antiradical nature of the samples was studied to explore their abilities relative to the standard with an expectation of developing active molecules against radical species. The data are concluded in Table 3 and related to a standard as displayed in Figure 17.

From the results concluded in Table 3, the complex [Cu(L_1) (L_2)] showed the best potential with maximum scavenging activities than the ligands (60.4–63.7%) close to ascorbic acid, and the least activity (32.60%–40.34%) was achieved by L_1. The scavenging activities were roughly concentration dependent, as concentration raises, the activities were also raising. It can be also concluded from the table, that the complex possesses higher radical scavenging properties than the constituent ligands. This may be due to the electron-deficient nature of the metals compared to their ligands.

3.10. Molecular Docking Studies

3.10.1. The Binding Interaction Studies on S. aureus gyrase. The *S. aureus gyrase* is a crucial enzyme in bacteria species for its survival. It kept bacteria DNA from damage during copying and imitations of the DNA strands [30]. Hence, stopping and interrupting the function of this enzyme is vital to be considered as a target for the antibacterial drug test. Thus, under this investigation, docking studies were done to examine their interaction and configuration with *S. aureus gyrase* (Figures 18–20). The docking results were compared with trimethoprim (Table 4).

Table 4 presented the lowermost binding energy of the prepared samples on the bacterial enzyme was found between −8.0 and −8.4 kcal/mol. The [Cu(L_1) (L_2)] complex displays the best binding (−8.4 kcal/mol) affinity. Relative to trimethoprim which had a binding potential of −7.9 kcal/mol, the samples achieved good interaction affinities and similar interaction profiles with amino acid residues. The data also displayed important H-bonding with amino acid scums and several interactions on bacterial DNA. The [Cu(L_1) (L_2)] complex possesses more additional H-bonding interactions. The overall docking results obtained match with *in vitro* data. Hence, the compounds are able to be considered antibacterial drug candidates with few modifications.

Figures 18–20 depict the information discovered under Table 4 using 2D, 3D model binding, and a 3D ribbon, model on *S. aureus* gyrase. H-bonds were shown by green,

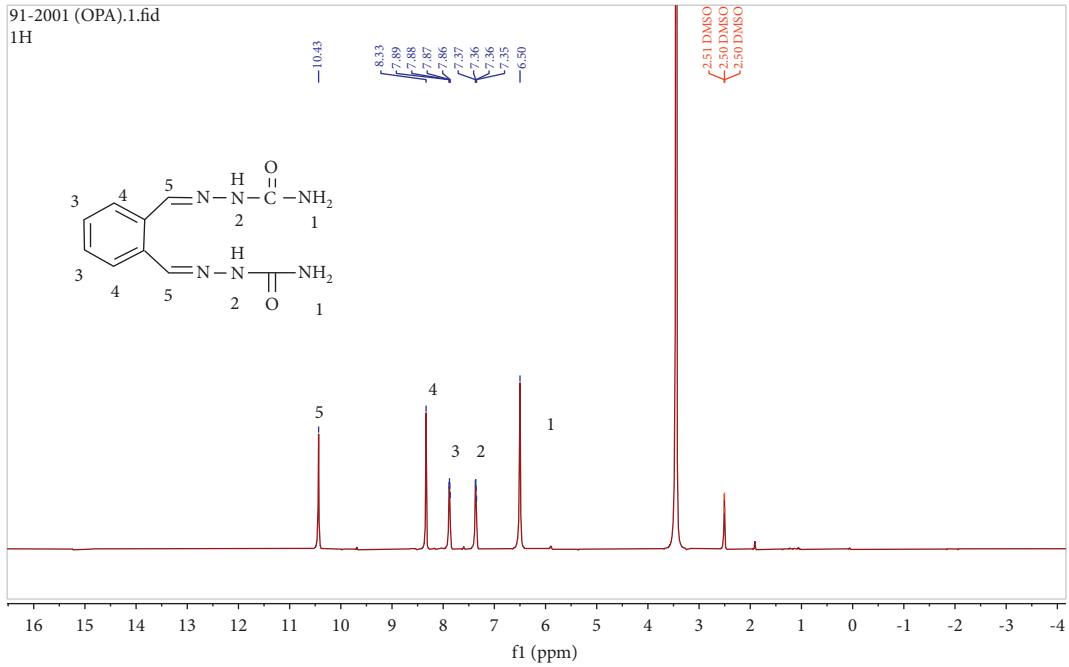

Figure 8: ^{1}H NMR spectra of L_1.

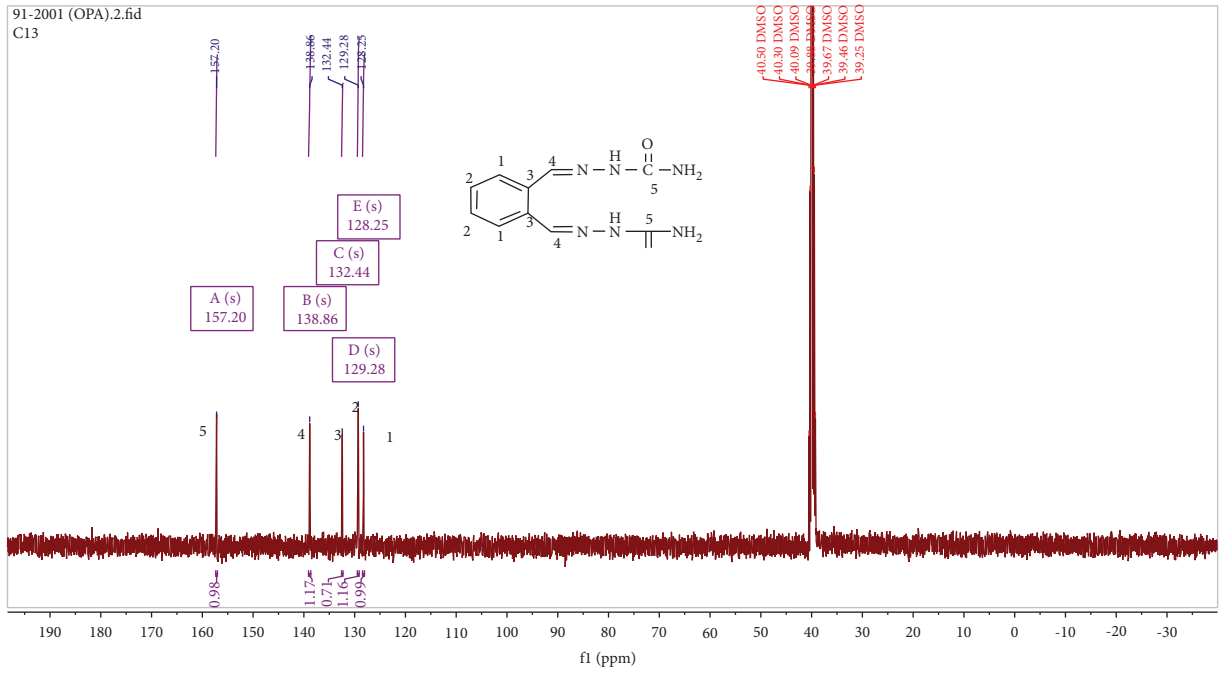

Figure 9: ^{13}C-NMR graphical spectra of L_1.

hydrophobic by pink, and pi-cation by orange colors, and the varied bonds that were induced between the samples and amino acids were shown by different colors.

3.10.2. The Binding Manner of Samples Docked against Myeloperoxidase. The binding manner of the samples put inside the sites of myeloperoxidase was investigated compared to ascorbic acid, see supplementary materials as shown in Figures S5, S6, and S7. It showed that the compounds show comparable binding nature (−7.9 to −9.5 kcal/mol) relative to vitamin C (−8.1 kcal/mol). The [Cu(L_1) (L_2)] complex and L_1 showed the best binding capability of −8.5

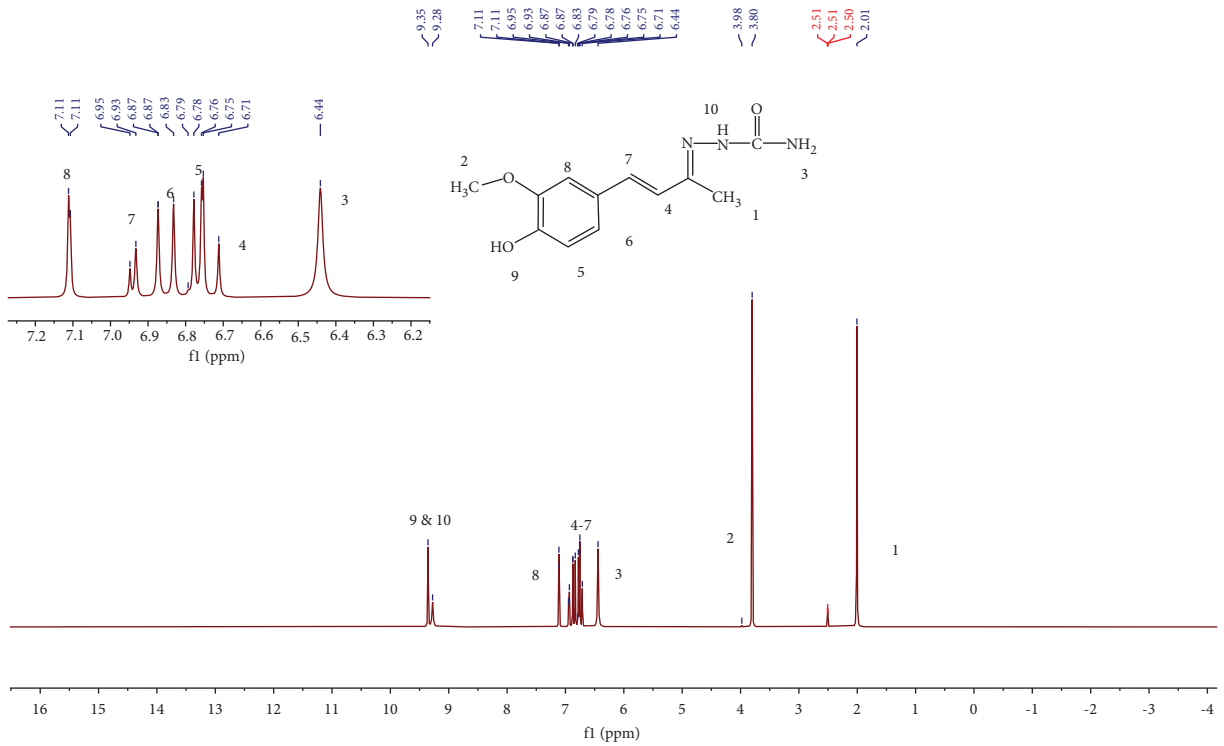

Figure 10: ^{1}H NMR graph of L_2.

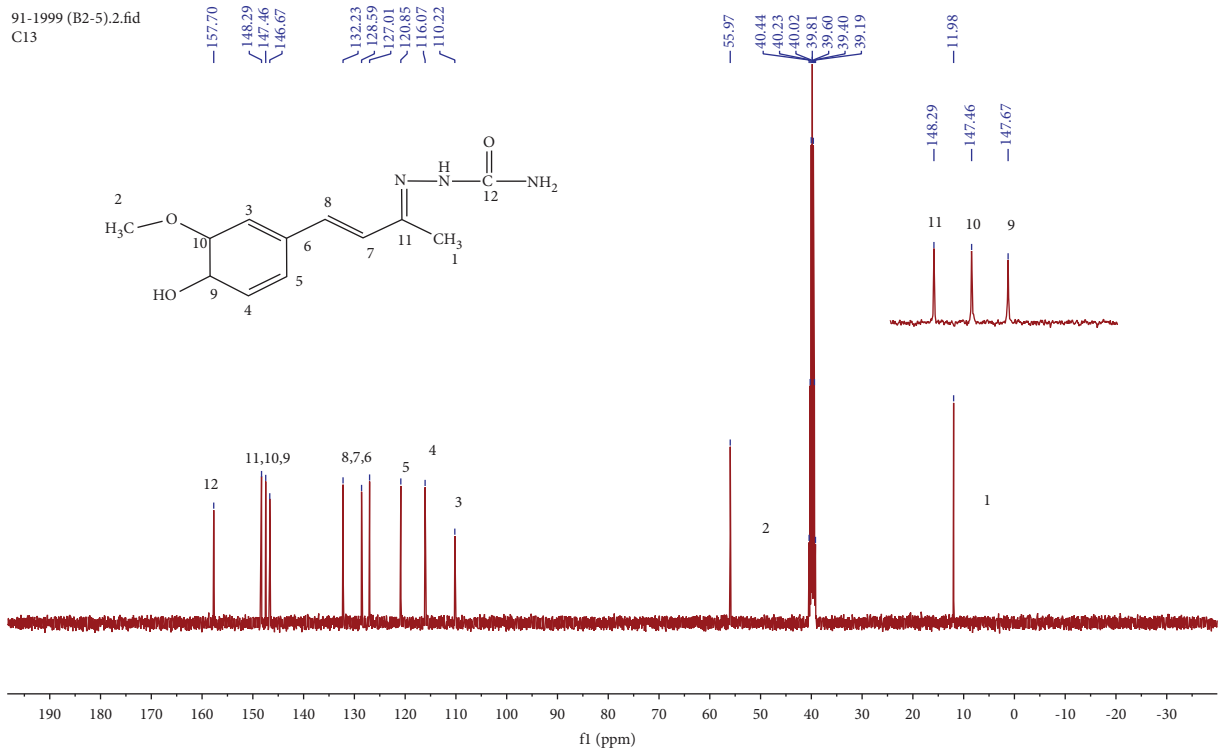

Figure 11: ^{13}C NMR graph of L_2.

and −9.5 kcal/mol orderly. The [Cu(L_1) (L_2)] complex has shown binding through hydrogen bonding with His-95, His-336, Thr-329, and Asp-98 residues similar to vitamin C (Table 5). The antiradical potential results were best correlated with the sample compounds that had good docking marks. As a result, the compounds could be useful as

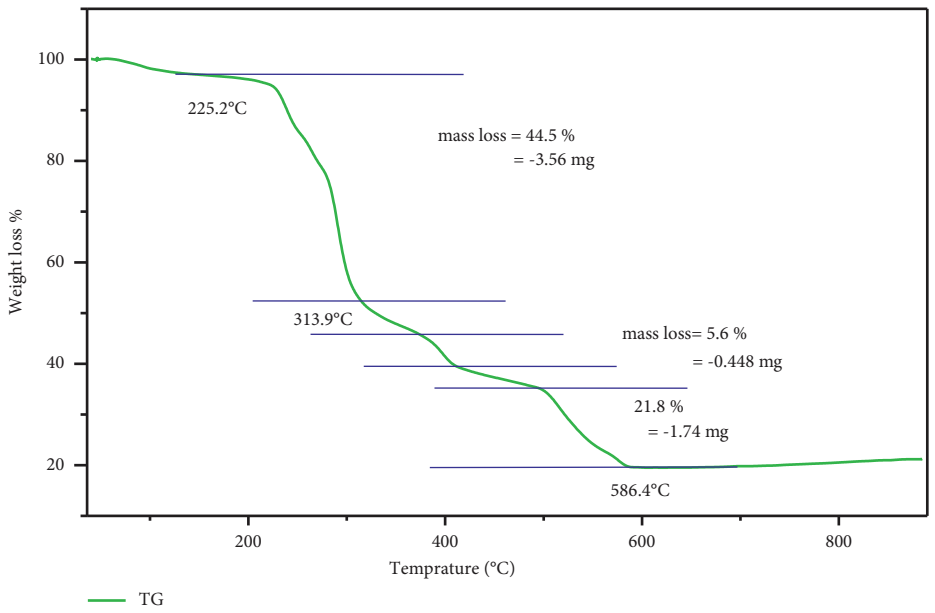

Figure 12: Thermogram curve of [Cu(L_1) (L_2)] complex.

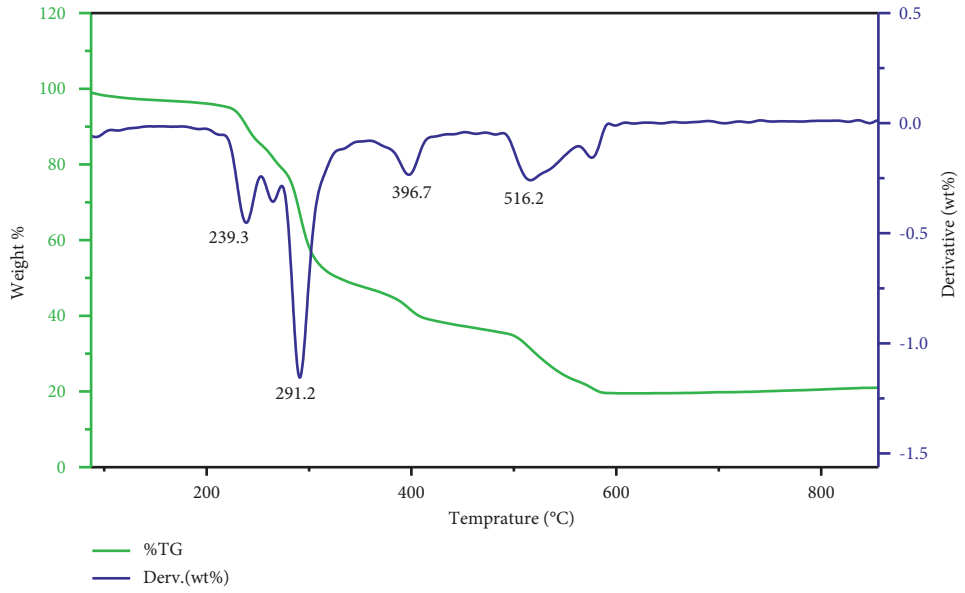

Figure 13: TG-DTG graph of [Cu(L_1) (L_2)] complex.

antiradical agents. Table 5 summarizes the information gathered and Figures S5–S7 (see supplementary materials) depicted the 2D, 3D mode of binding or 3D ribbon, and mark models.

3.10.3. Toxicity and Drug Similarity (Pharmacokinetics) Studies. If bioactive compounds meet "Lipinski's rule of five" [31], they are considered a promising drug candidate. As a result, the ligands' drug-likeness (pharmacokinetics) qualities were addressed by the rule. The criterion stipulates that prospective therapeutic compounds must have fewer than 10 H-bond acceptors (HBAs), fewer than 5 hydrogen-bond donors (HBDs), fewer than 5 log *P*, fewer than 500 Da molecular mass, and fewer than 140 Å overall polarity nature [32]. The results from the Swiss ADME workout (Table 6) demonstrate that the tested substances meet the criteria with zero violations.

Analyses of a compound's ADME are a crucial metric in the research of bioactive pharmacological agents. Tables 7 and 8 highlight the ADME features of the substances in comparison to the reference medications (trimethoprim and

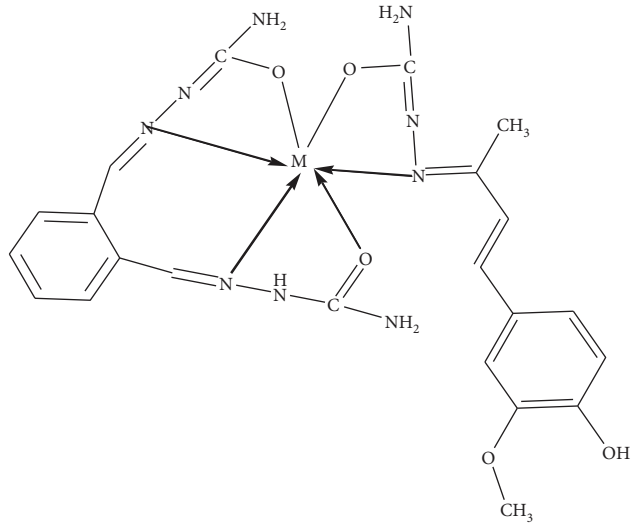

Figure 14: Proposed structures for [Cu(L_1) (L_2)] complex.

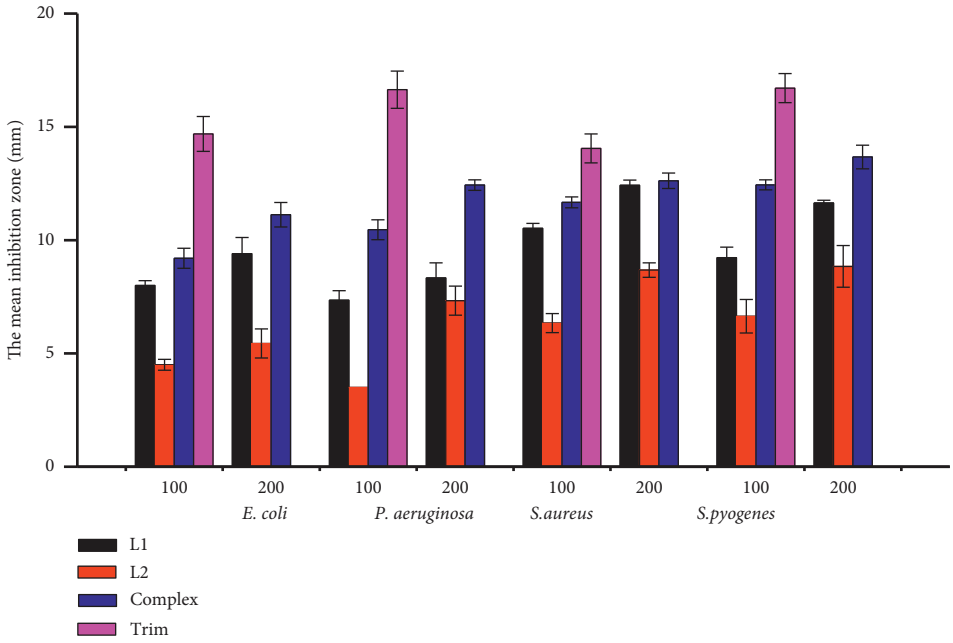

Figure 15: Inhibition zone plot of the samples on bacterial growth (mean ± SD).

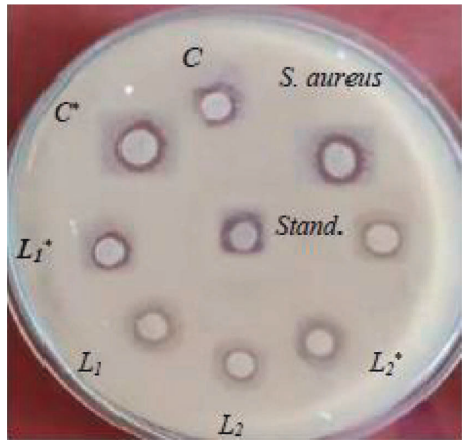

Figure 16: Distance moved by samples inhibiting the growth of *S. aureus*, where C and C ∗ and L and L ∗ are concentrations of the complex and ligands at 100 and 200 μg/mL, respectively.

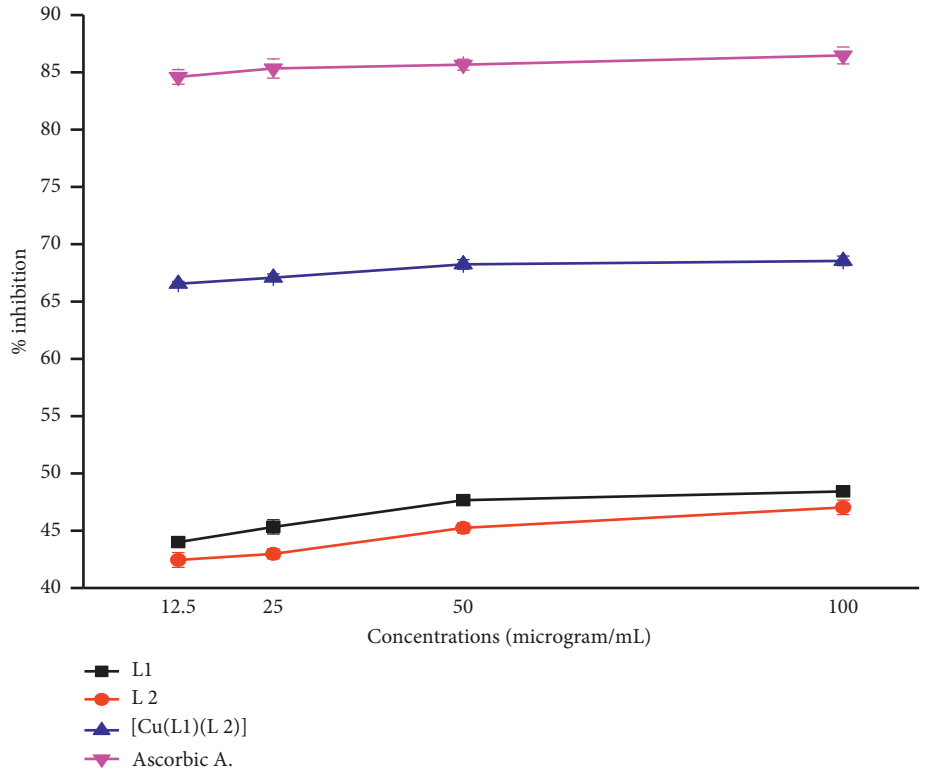

Figure 17: Antiradical potential (%) of samples relative to ascorbic acid.

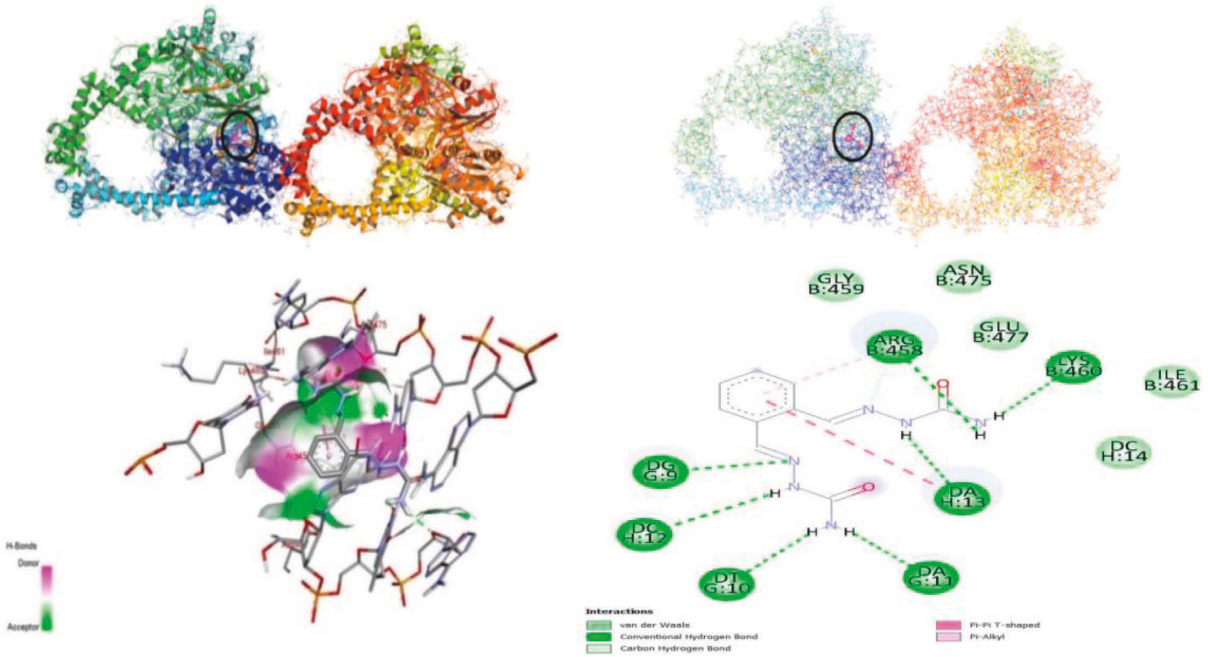

Figure 18: The L_1 binding to bacterium enzyme in two- and three-dimensional views.

ascorbic acid). The presence of a significant −log Kp value in the sample compounds confirms that they are not absorbed via the skin. L_1 had equivalent skin absorption to the trimethoprim (−8.33 and −8.54 cm/s); however, L_2 and [Cu(L_1) (L_2)] had greater skin fascination values (−7.15 and −7.45 cm/s). Moreover, both ligands and the [Cu(L_1) (L_2)] complex demonstrated substantial GI absorption but no BBB absorption.

Depending on toxicity classes (1 (toxic) to 6 (nontoxic)) and LD_{50} data found in Table 8, it can be confirmed that the samples did not show severe toxicity compared to the standard drugs. L_1 has displayed class 4 toxicity (not safe for

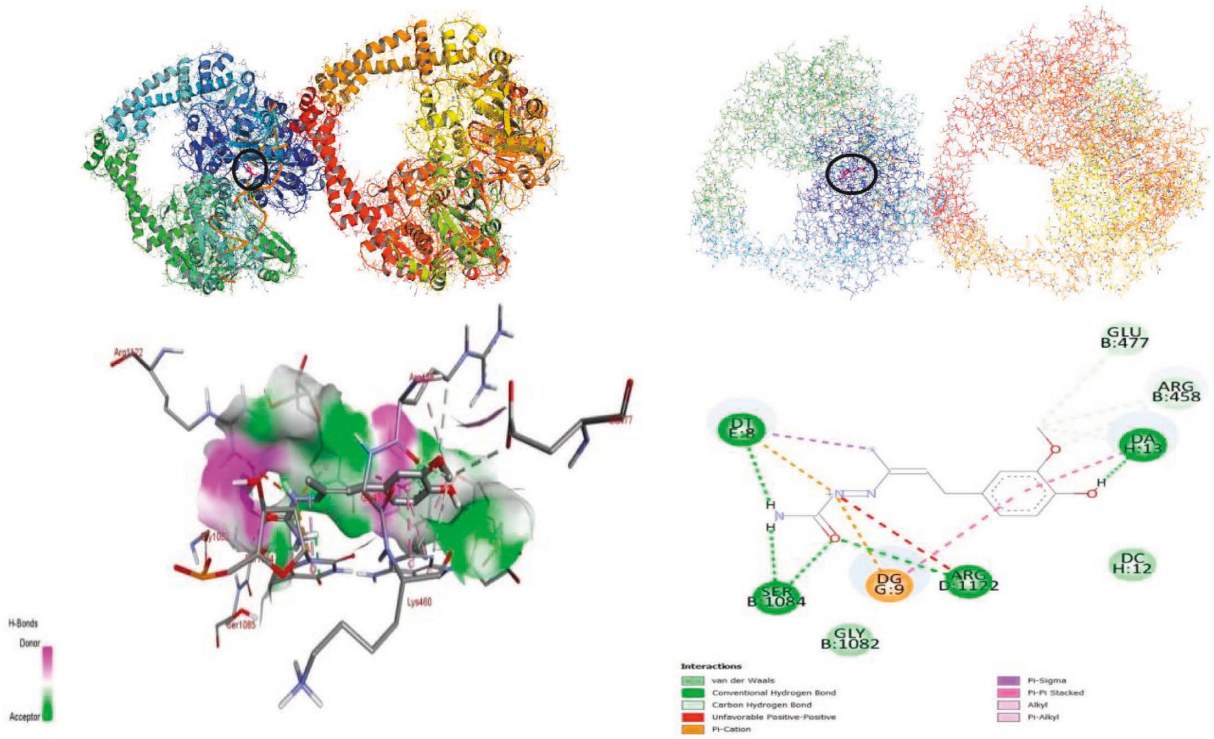

Figure 19: Shows the two- and three-dimensional binding modes of L_2 on *S. aureus gyrase*.

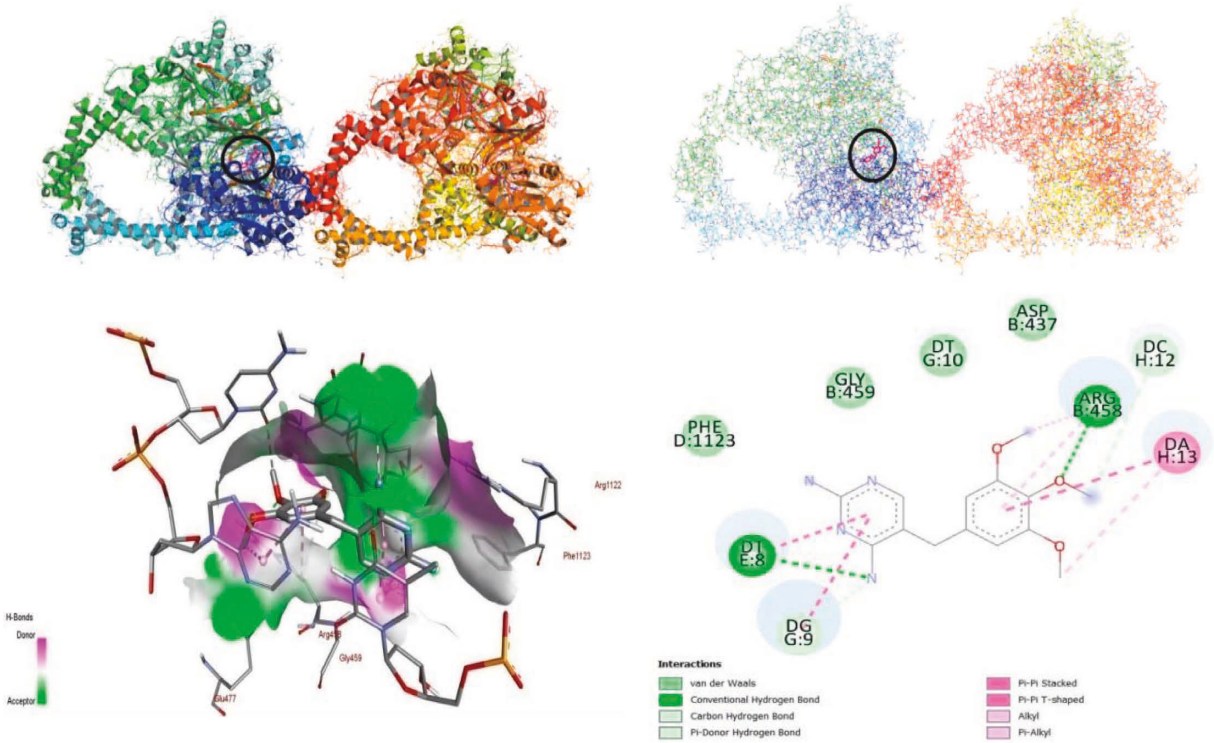

Figure 20: The two- and three-dimensional show of modes of binding by trimethoprim.

swallowing), and L_2 displayed better class 5 toxicity properties. Both ligands were considered noncytotoxic. Consequently, the compounds may be regarded as the top drug candidates based on the data analysis.

Table 4: The docking results of the samples on bacterial enzyme.

S. No.	Compounds	Binding affinities (kcal/mol	H-bonds	Residual interactions	
				Hydrophobic (pi-cation) and others	Van der Waals
1	L_1 $C_{10}H_{12}N_6O_2$	−8.2	Lys-460, Arg-458:O, Arg-458: CD, DG-9, DT-10, DA-11, DC-12, and DA-13	T-shaped-DA-13 Alkyl-Arg-458	Gly-459, Asn-475, Glu-477, Ile-461, and DC-14
2	L_2 $C_{12}H_{15}N_3O_3$	−8.0	Ser-1084: HG, Ser-1084: OG, Arg-458:CD, Arg-458:O, Arg-1122, Glu-477, DA13:N3, and DA-13: O4′ DT-8	Pi-cation-DT-8 electrostatic-pi-cation-DG-9 Pi-sigma-DT-8, pi-pi -DG-9, Pi-pi-DA-13(Dist. 4.12239 Å) Pi-pi -DA-13(Dist. 3.67512 Å) Alkyl-Arg-458, pi-Alkyl-DA-13(Dist. 5.19252 Å), and pi-Alkyl-DA-13(Dist. 4.36677 Å)	Gly-1082 and DG-12
3	[Cu(L_1) (L_2)] $C_{22}H_{25}N_9O_5Cu$	−8.4	Ser-438:HN, Ser-438: OG, Asp-1083 (Dist. 2.81399), Asp-1083 (Dist. 3.3489), DG-9: O6, and DG-9: N7	Pi-sigma-Ala-1120, pi-Sigma-Met-1121, Alkyl-Ala-1120, Alkyl-Met-1121, Alkyl-Arg-1122, and pi-Alkyl-Ala-1120	Tyr-1087, Ser-1084, Glu-1088, Ala-1118, Ala-1119, Gly-1117, Met-1075, and Phe-1123, Asp-437
	Trimethoprim $C_{14}H_{18}N_4O_3$	−7.9	Arg-458: DT-8,HH11, Arg-458: DG-9, CD, and DC-12	Pi-pi-DT-8, pi-pi -DG-9, pi-pi T-Shaped-DA-13, Alkyl-Arg-458, and pi-Alkyl-Arg-458 Pi-Alkyl-DA-13	Phe-1123, Gly-459, Asp-437, and DT-10

DA = deoxyadenosine, DT = deoxythymidine, DG = deoxyguanosine, and DC = Deoxycytidine.

Table 5: docking result of the sample on human myeloperoxidase.

S. No.	Compounds	Binding affinities (kcal/mol)	H-bonds	Residual interactions	
				Hydrophobic (pi-cation) and others	Van der Waals
1	L_1 $C_{10}H_{12}N_6O_2$	−7.9	Gly-155, Ser-156, Arg-161, Arg-148, Ser-42, and Cso-151	Pi-cation-Arg-148, electrostatic-pi-cation-Arg-161, pi-Alkyl-pro-123, and pi-Alkyl-Arg-148	Leu-43, Trp-47, Pro-124, Pro-103, Glu-102, Ser-149, Pro-151, Pro-154, and Cys-153
2	L_2 $C_{12}H_{15}N_3O_3$	−8.5	Arg-333, Asp-94, Asp-98, Gly-335:CA, Tyr-296, Phe-332, and Gly-335	Electrostatic-Asp-94, attractive charge-Asp-98, pi-Sulfur-Met-87 Amide-pi-GLY-90:C; GLN-91: N Pi-Alkyl-Phe-332, and pi-Alkyl-Tyr-334	Thr-329, His-95, Ile-339, Arg-239, His-336, Gln-91, and Leu-338
3	[Cu(L_1) (L_2)] $C_{22}H_{25}N_9O_5Cu$	−9.5	Gln-91, Arg-333: Arg-333: HH12 Arg-333: HH22, Arg-424, Thr-100, Thr-100, and Glu-242	Asp-94, Arg-333, and Glu-102	Asp-98,, Phe-99, His-95, Phe-332, Arg-239, Thr-329, Pro-101, His-336,,Ile-339, His-428, Asn-421, Leu-420, Leu-406, Phe-147, Phe-407, Ala-104, and Glu-116
	Ascorbic acid ($C_6H_8O_6$	−8.1	Gln-91,, Arg-239, Arg-239, Arg-333, Thr-100, Arg-333, and Arg-333: CA	Electrostatic-pi-anion-Asp-94 Hydrophobic-pi-Alkyl-Arg-333	His-336, Phe-99, Phe-332, His-95, Thr-329, and Asp-98

Table 6: Drug-likeness analysis of L_1 and L_2 estimation by Swiss ADME.

S. No.	Ligands	Mass (g/mol)	NHD	NHA	NRB	TPSA (Å^2)	Log*P* (iLOGP) lipophilicity	Log*S* (ESOL) water solubility	Synthetic convenience	Lipinski's rule (zero violations)
1	L_1	248.24	4	4	6	134.96	−0.43	−0.78	2.37	0
2	L_2	249.27	3	4	5	96.94	1.42	−1.90	2.80	0
	[Cu(L_1) (L_2)	559.01	4	4	5	102.6	1.46	−2.05	3.05	0
3	Trimethoprim	290.32	2	5	5	105.51	2.21	−2.31	2.58	0
	Ascorbic acid	176.12	4	6	2	107.22	−0.31	0.23	3.47	0

(NHD) = number of hydrogen donors, (NRB) = number of rotatable bonds, (NHA) = number of hydrogen acceptors, and (TPSA) = total polar surface area.

Table 7: ADME expectations worked out by Swiss ADME and preADMET.

S. No.	Ligands	SPV (LogKp) cm/s	GIA	BBBp	Pgps	Inhibitor interactions				
						CYP1A2 inhibitor	CYP2C19 inhibitor	CYP2C9 inhibitor	CYP2D6 inhibitor	CYP3A4 inhibitor
1	L_1	−8.33	High	No	No	No	No	No	No	No
2	L_2	−7.15	High	No	No	No	No	No	No	No
	[Cu(L_1) (L_2)	−7.45	High	No	No	No	No	No	No	No
3	Trimethoprim	−7.42	High	No	Yes	No	No	No	No	No
	Ascorbic acid	−8.54	High	No	No	No	No	No	No	No

SPV = skin permeability value, CYP = cytochrome-P, BBB = blood brain barrier permeability, GIA = gastrointestinal, and P-gp = P-glycoprotein substrate.

Table 8: Toxicity properties.

S. No.	Compounds	LD_{50} (mg/kg)	Toxicity classes	Organ toxicity					
				Hepatotoxicity	Carcinogenicity	Immunotoxicity	Mutagenicity	Cytotoxicity	Irritant
1	L_1	500	4	Active	Active	Inactive	Active	Inactive	No
2	L_2	1560	5	Active	Active	Active	Active	Inactive	No
	[Cu(L_1) (L_2)	2000	4	Inactive	Inactive	Inactive	Inactive	Inactive	No
3	Trimethoprim	3500	5	Inactive	Active	Active	Inactive	Inactive	No
	Ascorbic acid	3367	5	Inactive	Inactive	Inactive	Inactive	Inactive	No

4. Conclusions

Semicarbazone-based derivatives from synthetic and natural sources are effective scaffolds for developing bioactive ligands that can form stable complexes with metals. Both ligands form a complex with copper via nitrogen (-C=N) and carbonyl oxygen (-C=O) atoms. The geometrical configurations of [Cu(L_1) (L_2)] appear to be octahedral based on electronic (UV-vis) spectra information and the magnetic moment of a complex. Furthermore, conductivity results for the [Cu(L_1) (L_2)] complex indicate values of less than $60\ \Omega^{-1}\cdot cm^2\cdot mol^{-1}$, indicating that the complex generated was neutral, possessing no free anions outside the complex sphere. Within similar examination conditions, the antimicrobial potential data demonstrates that the [Cu(L_1) (L_2)] complex has a stronger antibacterial and antioxidant action potential than both constituent ligands. Compounds having good binding affinity, zero violations of Lipinski's assertion, and best coherence with antibacterial and antioxidant assay results in vitro were discovered using docking and drug-likeness ADME data. As a result, the ligands and the complex show a promise as antibacterial and antioxidant chemicals, with potential to be further refined for use as therapeutic molecules.

Data Availability

The data are included in the manuscript.

Conflicts of Interest

The authors declare that they have no conflicts of interest.

Acknowledgments

The authors would like to acknowledge Wolaita Sodo University and Adama Science and Technology University for technical as well as material support.

Supplementary Materials

Figure S1: the UV-Vis graph of L_1, Figure S2: the UV-Vis graph of L_2, Figure S3: the UV-Vis graph of the [Cu(L_1) (L_2)] complex, Figure S4: the XRD pattern of the Copper (II) complex, Figure S5: the 2D and 3D binding sites of L_1, Figure S6: the 2D and 3D binding mode of compound L_2, and Figure S7: the 2D and 3D binding mode of reference drug ascorbic acid. (*Supplementary Materials*)

References

[1] S. M. Dawoud, "Synthesis and DNA binding study of Co (II) and V (IV) complexes with O, N, O tridentate 3-methoxysalicylaldehyde-semicarbazide based ligand," *Journal of Physics: Conference Series*, vol. 1879, no. 2, Article ID 022059, 2021.

[2] D. Sarker, M. R. Karim, M. M. Haque, R. Zamir, and M. A. Asraf, "Copper (II) complex of salicylaldehyde semicarbazone: synthesis, characterization and antibacterial activity," *Asian Journal of Chemical Sciences*, vol. 6, no. 4, pp. 1–8, 2019.

[3] A. H. El-Ghorab, M. Nauman, F. M. Anjum, S. Hussain, and M. Nadeem, "A comparative study on chemical composition and antioxidant activity of ginger (Zingiber officinale) and cumin (Cuminum cyminum)," *Journal of Agricultural and Food Chemistry*, vol. 58, no. 14, pp. 8231–8237, 2010.

[4] A. Choudhary, R. Sharma, M. Nagar, M. Mohsin, and H. S. Meena, "Synthesis, characterization and antioxidant activity of some transition metal complexes with terpenoid derivatives," *Journal of the Chilean Chemical Society*, vol. 56, no. 4, pp. 911–917, 2011.

[5] S. Ahmad, A. A. Isab, S. Ali, and A. R. Al-Arfaj, "Perspectives in bioinorganic chemistry of some metal based therapeutic agents," *Polyhedron*, vol. 25, no. 7, pp. 1633–1645, 2006.

[6] E. Bahojb Noruzi, B. Shaabani, S. Geremia, N. Hickey, P. Nitti, and H. S. Kafil, "Synthesis, crystal structure, and biological activity of a multidentate calix [4] arene ligand doubly functionalized by 2-hydroxybenzeledene-thiosemicarbazone," *Molecules*, vol. 25, no. 2, p. 370, 2020.

[7] R. Deluchat, "Synthesis of 1, 4-diethynylbenzene," *Annali di Chimica*, vol. 11, no. 1, p. 181, 1934.

[8] C. Simons, S. E. Walsh, J. Y. Maillard, and A. D. Russell, "A note: ortho-phthalaldehyde: proposed mechanism of action of a new antimicrobial agent," *Letters in Applied Microbiology*, vol. 31, no. 4, pp. 299–302, 2000.

[9] R. M. Cabrera-Martinez, B. Setlow, and P. Setlow, "Studies on the mechanisms of the sporicidal action of ortho-phthalaldehyde," *Journal of Applied Microbiology*, vol. 92, no. 4, pp. 675–680, 2002.

[10] M. Simões, L. C. Simões, S. Cleto, I. Machado, M. O. Pereira, and M. J. Vieira, "Antimicrobial mechanisms of ortho-phthalaldehyde action," *Journal of Basic Microbiology*, vol. 47, no. 3, pp. 230–242, 2007.

[11] S. Yogosawa, Y. Yamada, S. Yasuda, Q. Sun, K. Takizawa, and T. Sakai, "Dehydrozingerone, a structural analogue of curcumin, induces cell-cycle arrest at the G2/M phase and accumulates intracellular ROS in HT-29 human colon cancer cells," *Journal of Natural Products*, vol. 75, no. 12, pp. 2088–2093, 2012.

[12] G. A. Hampannavar, R. Karpoormath, M. B. Palkar, and M. S. Shaikh, "An appraisal on recent medicinal perspective of curcumin degradant: dehydrozingerone (DZG)," *Bioorganic & Medicinal Chemistry*, vol. 24, no. 4, pp. 501–520, 2016.

[13] A. Awasthi, M. Lohani, M. K. Singh, A. T. Singh, and M. Jaggi, "Pharmacokinetic evaluation of C-3 modified 1, 8-naphthyridine-3-carboxamide derivatives with potent anticancer activity: lead finding," *Journal of Enzyme Inhibition and Medicinal Chemistry*, vol. 29, no. 5, pp. 710–721, 2014.

[14] A. Daina, O. Michielin, and V. Zoete, "SwissADME: a free web tool to evaluate pharmacokinetics, drug-likeness and medicinal chemistry friendliness of small molecules," *Scientific Reports*, vol. 7, no. 1, pp. 42717–42813, 2017.

[15] P. Banerjee, A. O. Eckert, A. K. Schrey, and R. Preissner, "ProTox-II: a webserver for the prediction of toxicity of chemicals," *Nucleic Acids Research*, vol. 46, no. W1, pp. W257–W263, 2018.

[16] A. Garg, A. Tadesse, and R. Eswaramoorthy, "A four-component domino reaction: an eco-compatible and highly efficient construction of 1, 8-naphthyridine derivatives, their in silico molecular docking, drug likeness, ADME, and toxicity studies," *Journal of Chemistry*, vol. 2021, Article ID 5589837, 16 pages, 2021.

[17] O. Trott and A. J. Olson, "AutoDock Vina: improving the speed and accuracy of docking with a new scoring function, efficient optimization, and multithreading," *Journal of Computational Chemistry*, vol. 31, no. 2, pp. 455–461, 2010.

[18] S. Goel, S. Chandra, and S. D. Dwivedi, "Synthesis, spectral and biological studies of copper (II) and iron (III) complexes derived from 2-acetyl benzofuran semicarbazone and 2-acetyl benzofuran thiosemicarbazone," *Journal of Saudi Chemical Society*, vol. 20, no. 6, pp. 651–660, 2016.

[19] F. Muleta, T. Desalegn, R. Eswaramoorthy, and A. Garg, "Synthesis, characterization, *in-silico*, and *in-vitro* biological studies of Cu (II), Zn (II) complexes of semicarbazone, thiosemicarbazone derivatives of dehydrozingerone," *Journal of Molecular Structure*, vol. 1268, Article ID 133632, 2022.

[20] M. Balouiri, M. Sadiki, and S. K. Ibnsouda, "Methods for *in vitro* evaluating antimicrobial activity: a review," *Journal of Pharmaceutical Analysis*, vol. 6, no. 2, pp. 71–79, 2016.

[21] S. Dutta, S. Padhye, K. I. Priyadarsini, and C. Newton, "Antioxidant and antiproliferative activity of curcumin semicarbazone," *Bioorganic & Medicinal Chemistry Letters*, vol. 15, no. 11, pp. 2738–2744, 2005.

[22] R. H. Holm, G. W. Everett, A. Chakravorty, and Chakravorty, "Metal complexes of Schiff bases and β-ketoamines," *Progress in Inorganic Chemistry*, vol. 7, pp. 83–214, 2007.

[23] W. J. Geary, "The use of conductivity measurements in organic solvents for the characterisation of coordination compounds," *Coordination Chemistry Reviews*, vol. 7, no. 1, pp. 81–122, 1971.

[24] F. K. Ommenya, "Synthesis, characterization and antibacterial activity of schiff base, 4-Chloro-2-{(E)-[(4-Fluorophenyl) imino] methyl} phenol and its transition metal (II) complexes," *Journal of Chemistry*, vol. 2020, Article ID 1745236, 8 pages, 2020.

[25] L. K Abdul Karem and S. H Mahdi, "Synthesis, spectral and biochemical studies of new complexes of mixed ligand Schiff base and anthranilic acid," *Oriental Journal of Chemistry*, vol. 34, no. 3, pp. 1565–1572, 2018.

[26] A. M. Shaker, L. AE. Nassr, M. S. S. Adam, and I. M. A. Mohamed, "Hydrophilicity and acid hydrolysis of water-soluble antibacterial iron (II) Schiff base complexes in binary aqueous solvents," *Russian Journal of General Chemistry*, vol. 83, no. 12, pp. 2460–2464, 2013.

[27] S. L. Reddy, T. Endo, and G. S. Reddy, "Electronic (absorption) spectra of 3D transition metal complexes," *Advanced aspects of spectroscopy*, vol. 1, no. 1, pp. 4–48, 2012.

[28] M. Alias, H. Kassum, and C. Shakir, "Synthesis, physical characterization and biological evaluation of Schiff base M (II) complexes," *Journal of the Association of Arab Universities for Basic and Applied Sciences*, vol. 15, no. 1, pp. 28–34, 2014.

[29] S. A. Andres, K. Bajaj, N. S. Vishnosky et al., "Synthesis, characterization, and biological activity of hybrid thiosemicarbazone– alkylthiocarbamate metal complexes," *Inorganic Chemistry*, vol. 59, no. 7, pp. 4924–4935, 2020.

[30] Z. Ghanbarimasir, A. Bekhradnia, K. Morteza-Semnani, A. Rafiei, N. Razzaghi-Asl, and M. Kardan, "Design, synthesis, biological assessment and molecular docking studies of new 2-aminoimidazole-quinoxaline hybrids as potential anticancer agents," *Spectrochimica Acta Part A: Molecular and Biomolecular Spectroscopy*, vol. 194, pp. 21–35, 2018.

[31] A. Mosa, A. A. Emara, J. M. Yousef, and A. A. Saddiq, "Novel transition metal complexes of 4-hydroxy-coumarin-3-thiocarbohydrazone: pharmacodynamic of Co (III) on rats and antimicrobial activity," *Spectrochimica Acta Part A: Molecular and Biomolecular Spectroscopy*, vol. 81, no. 1, pp. 35–43, 2011.

[32] A. Ah and A. Yi, "*In silico* pharmacokinetics and molecular docking studies of lead compounds derived from diospyros mespiliformis," *PharmaTutor*, vol. 7, no. 3, pp. 31–37, 2019.